Few-Body Systems manuscript No.
(will be inserted by the editor)

Jorge Segovia

Elastic and Transition Form Factors in DSEs

Received: / Accepted:

Abstract A symmetry preserving framework for the study of continuum Quantum Chromodynamics (QCD) is obtained from a truncated solution of the QCD equations of motion or QCD's Dyson-Schwinger equations (DSEs). A nonperturbative solution of the DSEs enables the study of, e.g., hadrons as composites of dressed-quarks and dressed-gluons, the phenomena of confinement and dynamical chiral symmetry breaking (DCSB), and therefrom an articulation of any connection between them. It is within this context that we present a unified study of Nucleon, Delta and Roper elastic and transition form factors, and compare predictions made using a framework built upon a Faddeev equation kernel and interaction vertices that possess QCD-like momentum dependence with results obtained using a symmetry-preserving treatment of a vector $\otimes$ vector contact-interaction.

Keywords Dyson-Schwinger equations · elastic and transition electromagnetic form factors · nucleon resonances

1 Introduction

Nonperturbative QCD poses significant challenges. Primary amongst them is a need to chart the behaviour of QCD's running coupling and masses into the domain of infrared momenta. Contemporary theory is incapable of solving this problem alone but a collaboration with experiment holds a promise for progress. This effort can benefit substantially by exposing the structure of nucleon excited states and measuring the associated transition form factors at large momentum transfers [1]. Large momenta are needed in order to pierce the meson-cloud that, often to a significant extent, screens the dressed-quark core of all baryons [2; 3]; and it is via the Q^2 evolution of form factors that one gains access to the running of QCD's coupling and masses from the infrared into the ultraviolet [4; 5].

A unified QCD-based description of elastic and transition form factors involving the nucleon and its resonances has acquired additional significance owing to substantial progress in the extraction of transition electrocouplings, $g_{\text{v}NN^*}$, from meson electroproduction data, obtained primarily with the CLAS detector at the Thomas Jefferson National Accelerator Facility (JLab). The electrocouplings of all low-lying N^* states with mass less-than 1.6 GeV have been determined via independent analyses of $\pi^+ n$, $\pi^0 p$ and $\pi^+\pi^- p$ exclusive channels [6; 7]; and preliminary results for the $g_{\text{v}NN^*}$ electrocouplings of most high-lying N^* states with masses below 1.8 GeV have also been obtained from CLAS meson electroproduction data [1; 8].

Jorge Segovia
Instituto Universitario de Física Fundamental y Matemáticas (IUFFyM)
Universidad de Salamanca
Plaza de la Merced 1-4, 37008 Salamanca, Spain
Tel.: +34-923-294434
Fax: +34-923-294584
E-mail: segonza@usal.es

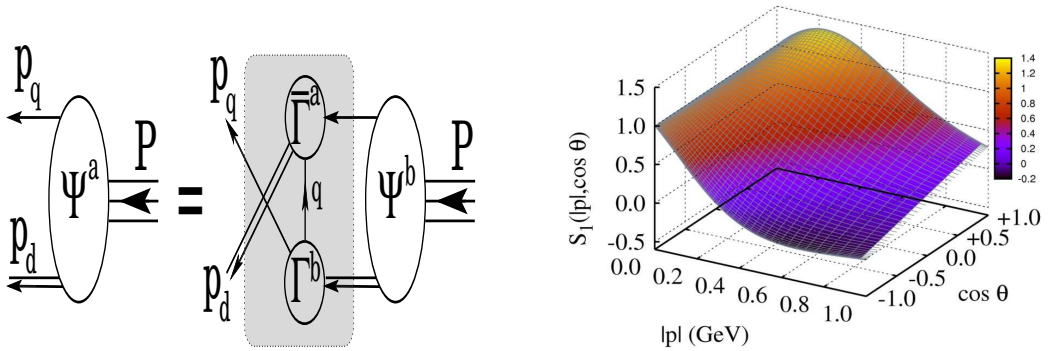

Fig. 1 *Left panel:* Poincaré covariant Faddeev equation. Ψ is the Faddeev amplitude for a baryon of total momentum $P = p_q + p_d$, where $p_{q,d}$ are, respectively, the momenta of the quark and diquark within the bound-state. The shaded area demarcates the Faddeev equation kernel: *single line*, dressed-quark propagator; Γ, diquark correlation amplitude; and *double line*, diquark propagator. *Right panel:* Dominant piece in the nucleon's eight-component Poincaré-covariant Faddeev amplitude: $S_1(|p|,\cos\theta)$. In the nucleon rest frame, this term describes that piece of the quark–scalar-diquark relative momentum correlation which possesses zero intrinsic quark-diquark orbital angular momentum, i.e. $L = 0$ before the propagator lines are reattached to form the Faddeev wave function. Referring to Fig. 1, $p = P/3 - p_q$ and $\cos\theta = p \cdot P/\sqrt{p^2 P^2}$. The amplitude is normalised such that its U_0 Chebyshev moment is unity at $|p| = 0$.

Many new insights have been revealed in a series of recent articles [9; 10; 11; 12; 13] focused on the calculation of the Nucleon, Delta and Roper elastic and transition form factors using a widely-used leading-order (rainbow-ladder) truncation of QCD's Dyson-Schwinger equations and comparing results between a QCD-based framework and a vector $\otimes$ vector contact interaction. It is our purpose here reviewing some of the most important outcomes and refer to the interested reader to the original works for details.

2 Baryon structure

The existence of strong diquark correlations inside baryons is a dynamical prediction of Faddeev equation studies based on the observation that the attractive nature of quark-antiquark correlations in a colour-singlet meson is also attractive for $\bar{3}_c$ quark-quark correlations within a colour-singlet baryon [14].

In the quark+diquark picture, baryons are described by the Poincaré covariant Faddeev equation depicted in the left panel of Fig. 1. Two main contributions appear in the binding energy: i) the formation of tight diquark correlations and ii) the quark exchange depicted in the shaded area of the left panel of Fig. 1[1]. This exchange ensures that diquark correlations within the baryon are fully dynamical: no quark holds a special place because each one participates in all diquarks to the fullest extent allowed by its quantum numbers. Attending to the quantum numbers of the nucleon and Roper, scalar and pseudovector diquark correlations are dominant whereas only pseudovector ones are present inside the Δ-baryon.

The quark+diquark structure of the nucleon is elucidated in the right panel of Fig. 1, which depicts the leading component of its Faddeev amplitude: with the notation of Ref. [11], $S_1(|p|,\cos\theta)$, computed using the Faddeev kernel described therein. This function describes a piece of the quark+scalar-diquark relative momentum correlation. Notably, in this solution of a realistic Faddeev equation there is strong variation with respect to both arguments. Support is concentrated in the forward direction, $\cos\theta > 0$, so that alignment of p and P is favoured; and the amplitude peaks at $(|p| \simeq M_N/6, \cos\theta = 1)$, whereat $p_q \sim p_d \sim P/2$ and hence the natural relative momentum is zero. In the antiparallel direction, $\cos\theta < 0$, support is concentrated at $|p| = 0$, i.e. $p_q \sim P/3$, $p_d \sim 2P/3$.

The strong diquark correlations must be evident in many physical observables. We focus our attention on the flavour separated versions of the Dirac a Pauli form factors of the nucleon. Figure 2 displays the proton's flavour separated Dirac and Pauli form factors. The salient features of the data are: the d-quark contribution to F_1^p is far smaller than the u-quark contribution; $F_2^d/\kappa_d > F_2^u/\kappa_u$ on $x < 2$ but this ordering is reversed on $x > 2$; and in both cases the d-quark contribution falls

[1] Whilst an explicit three-body term might affect fine details of baryon structure, the dominant effect of non-Abelian multi-gluon vertices is expressed in the formation of diquark correlations [15].

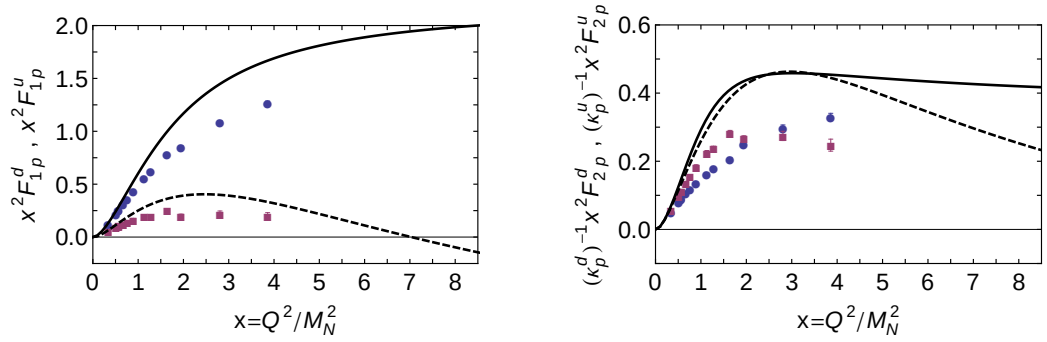

Fig. 2 *Left panel:* Flavour separation of the proton's Dirac form factor as a function of $x = Q^2/M_N^2$. The results have been obtained using a framework built upon a Faddeev equation kernel and interaction vertices that possess QCD-like momentum dependence. The solid-curve is the u-quark contribution, and the dashed-curve is the d-quark contribution. Experimental data taken from Ref. [16] and references therein: circles – u-quark; and squares – d-quark. *Right panel:* Same for Pauli form factor.

dramatically on $x > 3$ whereas the u-quark contribution remains roughly constant. Our calculations are in semi-quantitative agreement with the empirical data.

It is natural to seek an explanation for the pattern of behaviour in Fig. 2. We have mentioned that the proton contains scalar and pseudovector diquark correlations. The dominant piece of its Faddeev wave function is $u[ud]$; namely, a u-quark in tandem with a $[ud]$ scalar correlation, which produces 62% of the proton's normalisation. If this were the sole component, then photon–d-quark interactions within the proton would receive a $1/x$ suppression on $x > 1$, because the d-quark is sequestered in a soft correlation, whereas a spectator u-quark is always available to participate in a hard interaction. At large $x = Q^2/M_N^2$, therefore, scalar diquark dominance leads one to expect $F^d \sim F^u/x$. Available data are consistent with this prediction but measurements at $x > 4$ are necessary for confirmation.

3 The $\gamma^* N \to \Delta$ Transition

The electromagnetic $\gamma^* N \to \Delta$ transition is described by three Poincaré-invariant form factors [17]: magnetic-dipole, G_M^*, electric quadrupole, G_E^*, and Coulomb (longitudinal) quadrupole, G_C^*; that can be extracted in the Dyson-Schwinger approach by a sensible set of projection operators [18]. The following ratios

$$R_{\rm EM} = -\frac{G_E^*}{G_M^*}, \qquad R_{\rm SM} = -\frac{|\mathbf{Q}|}{2m_\Delta}\frac{G_C^*}{G_M^*}, \tag{1}$$

are often considered because they can be read as measures of the deformation of the hadrons involved in the reaction and how such deformation influences the structure of the transition current.

The upper-left panel of Fig. 3 displays the magnetic transition form factor in the Jones-Scadron convention. Our prediction obtained with a QCD-based kernel agrees with the data on $x \gtrsim 0.4$, and a similar conclusion can be inferred from the contact interaction result. On the other hand, both curves disagree markedly with the data at infrared momenta. This is explained by the similarity between these predictions and the bare result determined using the Sato-Lee (SL) dynamical meson-exchange model [19]. The SL result supports a view that the discrepancy owes to omission of meson-cloud effects in the DSEs' computations. An exploratory study of the effect of pion-cloud contributions to the mass of the nucleon and the Δ-baryon has been performed within a DSEs' framework in Ref. [20].

Presentations of the experimental data associated with the magnetic transition form factor typically use the Ash convention. This comparison is depicted in the upper-right panel of Fig. 3. One can see that the difference between form factors obtained with the QCD-kindred and CI frameworks increases with the transfer momentum. Moreover, the normalized QCD-kindred curve is in fair agreement with the data, indicating that the Ash form factor falls unexpectedly rapidly mainly for two reasons. First: meson-cloud effects provide up-to 35% of the form factor for $x \lesssim 2$; these contributions are very soft; and hence they disappear quickly. Second: the additional kinematic factor $\sim 1/\sqrt{Q^2}$ that appears between Ash and Jones-Scadron conventions and provides material damping for $x \gtrsim 2$.

Our predictions for the ratios in Eq. (1) are depicted in the lower panels of Fig. 3. The left panel displays the Coulomb quadrupole ratio. Both the prediction obtained with QCD-like propagators

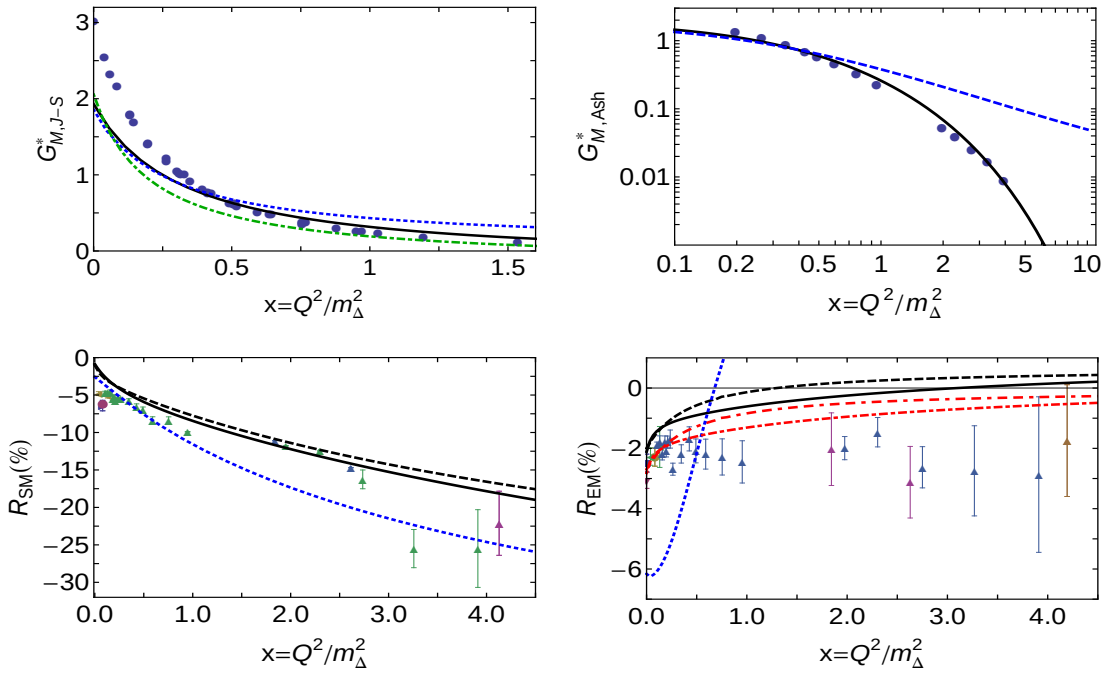

Fig. 3 *Upper-left panel* – $G^*_{M,J-S}$ result obtained with QCD-based interaction (solid, black) and with contact-interaction (CI) (dotted, blue); The green dot-dashed curve is the dressed-quark core contribution inferred using SL-model [19]. *Upper-right panel* – $G^*_{M,Ash}$ result obtained with QCD-based interaction (solid, black) and with CI (dotted, blue). *Lower-left panel* – R_{SM} prediction of QCD-based kernel including dressed-quark anomalous magnetic moment (DqAMM) (black, solid), nonincluding DqAMM (black, dashed), and CI result (dotted, blue). *Lower-right panel* – R_{EM} prediction obtained with QCD-kindred framework (solid, black); same input but without DqAMM (dashed, black); these results renormalised (by a factor of 1.34) to agree with experiment at $x = 0$ (dot-dashed, red - zero at $x \approx 14$; and dot-dash-dashed, red, zero at $x \approx 6$); and CI result (dotted, blue). The data in the panels are from references that can be found in [11].

and vertices and the contact-interaction result are broadly consistent with available data. This shows that even a contact-interaction can produce correlations between dressed-quarks within Faddeev wave-functions and related features in the current that are comparable in size with those observed empirically. Moreover, suppressing the dressed-quark anomalous magnetic moment (DqAMM) in the transition current has little impact. These remarks highlight that R_{SM} is not particularly sensitive to details of the Faddeev kernel and transition current.

This is certainly not the case with R_{EM}. The differences between the curves displayed in the lower-right panel in Fig. 3 show that this ratio is a particularly sensitive measure of diquark and orbital angular momentum correlations. The contact-interaction result is inconsistent with data, possessing a zero that appears at a rather small value of x. On the other hand, predictions obtained with QCD-like propagators and vertices can be viable. We have presented four variants, which differ primarily in the location of the zero that is a feature of this ratio in all cases we have considered. The inclusion of a DqAMM shifts the zero to a larger value of x. Given the uniformly small value of this ratio and its sensitivity to the DqAMM, we judge that meson-cloud affects must play a large role on the entire domain that is currently accessible to experiment.

4 The $\gamma^* N \to$ *Roper* Transition

Jefferson Lab experiments [22; 21; 23; 7] have yielded precise nucleon-Roper ($N \to R$) transition form factors and thereby exposed the first zero seen in any hadron form factor or transition amplitude. It has also attracted much theoretical attention; but Ref. [13] provides the first continuum treatment of this problem using the power of relativistic quantum field theory. That study begins with a computation of the mass and wave function of the proton and its first radial excitation. The masses are (in GeV): $M_{\mathrm{nucleon\,(N)}} = 1.18$ and $M_{\mathrm{nucleon-excited\,(R)}} = 1.73$. These values correspond to the locations

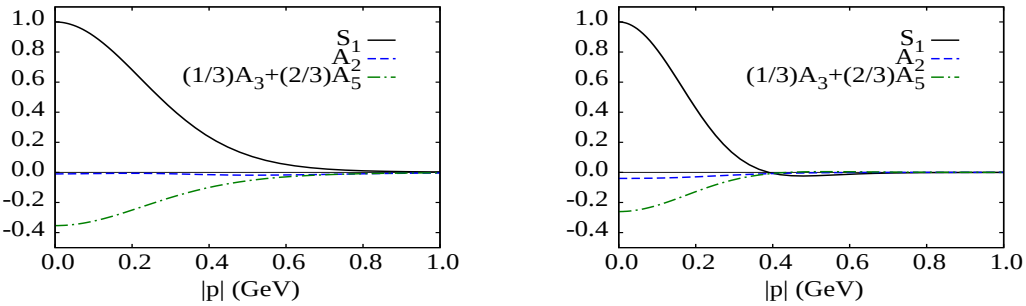

Fig. 4 *Left panel.* Zeroth Chebyshev moment of all S-wave components in the nucleon's Faddeev wave function. *Right panel.* Kindred functions for the first excited state. Legend: S_1 is associated with the baryon's scalar diquark; the other two curves are associated with the axial-vector diquark; and the normalisation is chosen such that $S_1(0) = 1$.

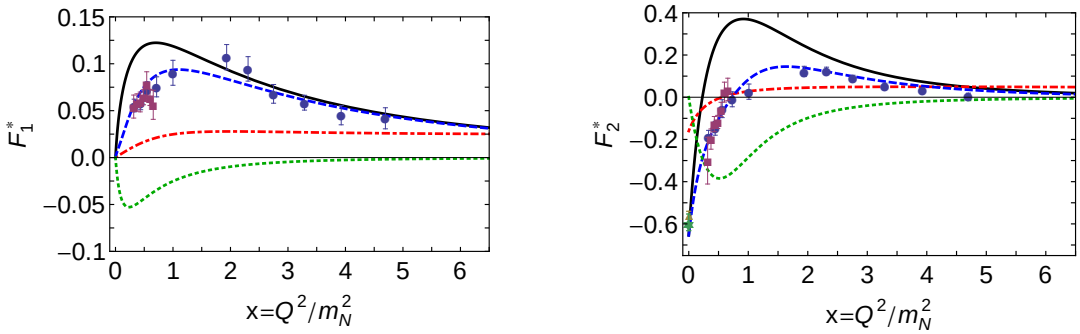

Fig. 5 *Left* – Dirac transition form factor, $F_1^*(x)$, $x = Q^2/m_N^2$. Solid (black) curve, QCD-kindred prediction; dot-dashed (red) curve, contact-interaction result; dotted (green) curve, inferred meson-cloud contribution; and dashed (blue) curve, anticipated complete result. *Right* – Pauli transition form factor, $F_2^*(x)$, with same legend. Data in both panels: circles (blue) [21]; triangle (gold) [23]; squares (purple) [7]; and star (green) [6].

of the two lowest-magnitude $J^P = 1/2^+$ poles in the three-quark scattering problem. The associated residues are the Faddeev wave functions, which depend upon $(p^2, p \cdot P)$, where p is the quark-diquark relative momentum. Fig. 4 depicts the zeroth Chebyshev moment of all S-wave components in that wave function. The appearance of a single zero in S-wave components of the Faddeev wave function associated with the first excited state in the three dressed-quark scattering problem indicates that this state is a radial excitation.

The empirical values of the pole locations for the first two states in the nucleon channel are [24]: 0.939 GeV and $1.36 - i\,0.091$ GeV, respectively. At first glance, these values appear unrelated to those obtained within the DSEs framework. However, deeper consideration reveals [25; 26] that the kernel in the Faddeev equation omits all those resonant contributions which may be associated with the meson-baryon final-state interactions that are resummed in dynamical coupled channels models in order to transform a bare-baryon into the observed state [24; 3]. This Faddeev equation should therefore be understood as producing the dressed-quark core of the bound-state, not the completely-dressed and hence observable object. Crucial, therefore, is a comparison between the quark-core mass and the value determined for the mass of the meson-undressed bare-Roper in Ref. [24] which is 1.76 GeV.

The transition form factors are displayed in Fig. 5. The results obtained using QCD-derived propagators and vertices agree with the data on $x \gtrsim 2$. The contact-interaction result simply disagree both quantitatively and qualitatively with the data. Therefore, experiment is evidently a sensitive tool with which to chart the nature of the quark-quark interaction and hence discriminate between competing theoretical hypotheses.

The mismatch between the DSE predictions and data on $x \lesssim 2$ is due to Meson-cloud contributions that are expected to be important on this domain. An inferred form of that contribution is provided by the dotted (green) curves in Fig. 5. These curves have fallen to just 20% of their maximum value by $x = 2$ and vanish rapidly thereafter so that the DSE predictions alone remain as the explanation of the data. Importantly, the existence of a zero in F_2^* is not influenced by meson-cloud effects, although its precise location is.

5 Conclusions

We described a unified study of Nucleon, Delta and Roper elastic and transition form factors that compares predictions made by a QCD-kindred framework with results obtained using a symmetry-preserving treatment of a vector $\otimes$ vector contact-interaction. The comparison emphasises that experiment is sensitive to the momentum dependence of the running coupling and masses in QCD. Amongst our results, the following are of particular interest: the presence of strong diquark correlations within the nucleon is sufficient to understand empirical extractions of the flavour-separated form factors. In connection with the $\gamma^* N \to \Delta$ transition, the momentum-dependence of the magnetic transition form factor, G_M^*, matches that of G_M^n once the momentum transfer is high enough to pierce the meson-cloud; and the electric quadrupole ratio is a keen measure of diquark and orbital angular momentum correlations, the zero in which is obscured by meson-cloud effects on the domain currently accessible to experiment. Finally, the Roper resonance is at heart of the nucleon's first radial excitation, consisting of a dressed-quark core augmented by a meson cloud that reduces its mass by approximately 20%. Our analysis shows that a meson-cloud obscures the dressed-quark core from long-wavelength probes, but that it is revealed to probes with $Q^2 \gtrsim 3m_N^2$.

Acknowledgements The material described in this contribution is drawn from work completed in collaboration with numerous excellent people, to all of whom I am greatly indebted. I would also like to thank V. Mokeev, R. Gothe, T.-S. H. Lee and G. Eichmann for insightful comments; and to express my gratitude to the organisers of the *Light Cone 2015*, whose support helped my participation. I acknowledges financial support from a postdoctoral IUFFyM contract at Universidad de Salamanca, Spain.

References

1. I.G. Aznauryan *et al.* (2013) Studies of Nucleon Resonance Structure in Exclusive Meson Electroproduction. Int. J. Mod. Phys. E22: 1330015.
2. C.D. Roberts (2011) Opportunities and Challenges for Theory in the N^* program. AIP Conf. Proc. 1432: 19–25.
3. H. Kamano *et al.* (2013) Nucleon resonances within a dynamical coupled-channels model of πN and γN reactions. Phys. Rev. C88: 035209.
4. I.C. Cloët *et al.* (2013) Revealing dressed-quarks via the proton's charge distribution. Phys. Rev. Lett. 111:101803.
5. L. Chang *et al.* (2013) Pion electromagnetic form factor at spacelike momenta. Phys. Rev. Lett. 111: 141802.
6. K.A. Olive *et al.* (Particle Data Group) (2014) The review of Particle Physics. Chin. Phys. C38: 090001.
7. V.I. Mokeev *et al.* (2012) Experimental Study of the $P_{11}(1440)$ and $D_{13}(1520)$ resonances from CLAS data on $ep \to e'\pi^+\pi^- p'$. Phys. Rev. C86: 035203.
8. V.I. Mokeev *et al.* (2013) Studies of N^* structure from the CLAS meson electroproduction data. Int. J. Mod. Phys. Conf. Ser. 26: 1460080.
9. J. Segovia *et al.* (2013) Insights into the $\gamma^* N \to \Delta$ transition. Phys. Rev. C88: 032201.
10. J. Segovia *et al.* (2013) Elastic and Transition Form Factors of the $\Delta(1232)$. Few Body Syst 55: 1–33.
11. J. Segovia *et al.* (2014) Nucleon and Δ elastic and transition form factors. Few Body Syst. 55: 1185-1222
12. J. Segovia *et al.* (2015) Understanding the nucleon as a Borromean bound-state. Phys. Lett. B750: 100–106.
13. J. Segovia *et al.* (2015) Completing the picture of the Roper resonance. Phys. Rev. Lett. 115: 171801.
14. R.T. Cahill *et al.* (1989) Baryon Structure and QCD. Austral. J. Phys. 42: 129–145.
15. G. Eichmann *et al.* (2010) Nucleon mass from a covariant three-quark Faddeev equation. Phys. Rev. Lett. 104: 201601.
16. G.D. Cates *et al.* (2011) Flavor decomposition of the elastic nucleon electromagnetic form factors. Phys. Rev. Lett. 106: 252003.
17. H.F. Jones *et al.* (1973) Multipole $\gamma N\Delta$ form-factors and resonant photoproduction and electroproduction. Annals Phys. 81: 1–14.
18. G. Eichmann *et al.* (2012) Nucleon to Delta electromagnetic transition in the Dyson-Schwinger approach. Phys. Rev. D85: 093004.
19. B. Julia-Diaz *et al.* (2007) Extraction and Interpretation of $\gamma N \to \Delta$ Form Factors within a Dynamical Model. Phys. Rev. C75: 015205.
20. H. Sanchis-Alepuz *et al.* (2014) Pion cloud effects on baryon masses. Phys. Lett. B733: 151–157.
21. I.G. Aznauryan *et al.* (2009) Electroexcitation of nucleon resonances from CLAS data on single pion electroproduction. Phys. Rev. C80: 055203.
22. I.G. Aznauryan *et al.* (2012) Electroexcitation of nucleon resonances. Prog. Part. Nucl. Phys. 67: 1–54.
23. M. Dugger *et al.* (2009) π^+ photoproduction on the proton for photon energies from 0.725 to 2.875 GeV. Phys. Rev. C79: 065206.
24. N. Suzuki *et al.* (2010) Disentangling the Dynamical Origin of P_{11} Nucleon Resonances. Phys. Rev. Lett. 104: 042302.
25. G. Eichmann *et al.* (2008) Perspective on rainbow-ladder truncation. Phys. Rev. C77: 042202.
26. G. Eichmann *et al.* (2009) Toward unifying the description of meson and baryon properties. Phys. Rev. C79:012202.